LBNL-42386

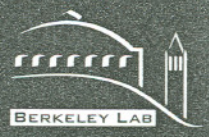

ERNEST ORLANDO LAWRENCE
BERKELEY NATIONAL LABORATORY

EOSHYDR: A TOUGH2 Module for CH_4-Hydrate Release and Flow in the Subsurface

George Moridis, John Apps,
Karsten Pruess, and Larry Myer

Earth Sciences Division

September 1998

Presented at
Methane Hydrates,
Chiba City, Japan,
October 20–22, 1998,
and to be published in
the Proceedings

LBNL-42386

EOSHYDR: A TOUGH2 MODULE FOR CH_4-HYDRATE RELEASE AND FLOW IN THE SUBSURFACE

**George Moridis, John Apps,
Karsten Pruess and Larry Myer**

*Earth Sciences Division
Lawrence Berkeley National Laboratory
Berkeley, CA 94720*

September 1998

This work was supported by the Director, Office of Science, of the U.S. Department of Energy under Contract No. DE-AC03-76SF00098.

EOSHYDR: A TOUGH2 Module for CH_4-Hydrate Release and Flow In the Subsurface

George Moridis, John Apps, Karsten Pruess and Larry Myer
Earth Sciences Division, Lawrence Berkeley National Laboratory, University of California, Berkeley, California

Abstract. EOSHYDR is a new module for the TOUGH2 general-purpose simulator for multi-component, multiphase fluid and heat flow and transport in the subsurface. EOSHYDR is designed to model the non-isothermal CH_4 release, phase behavior and flow under the conditions of the common methane hydrate deposits (i.e., in the permafrost and in deep ocean sediments) by solving the coupled equations of mass and heat balance. As with all other members of the TOUGH2 family of codes, EOSHYDR can handle multi-dimensional flow domains and cartesian, cylindrical or irregular grids, as well as porous and fractured media.

EOSHYDR extends the thermophysical description of water to temperatures as low as $-30\ ^0$C. Both an equilibrium and a kinetic model of hydrate formation or dissociation are included. Two new solid phases are introduced, one for the CH_4-hydrate and the other for ice. Under equilibrium conditions, water and methane, as well as heat, are the main components. In the kinetic model, the solid hydrate is introduced as the fourth component. The mass components are partitioned among the gas, liquid and the two solid phases. The thermodynamic phase equilibrium in EOSHYDR is described by the P-T-X diagram of the H_2O - CH_4 system. Phase changes and the corresponding heat transfers are fully described. The effect of salt in pore waters on CH_4 solubility and on the growth and decomposition of gas hydrates is also taken into account.

Results are presented for three test problems designed to explore different mechanisms and strategies for production from CH_4-hydrate reservoirs. These tests include thermal

stimulation and depressurization under both permafrost and suboceanic conditions. The results of the tests tend to indicate that CH_4 production from CH_4-hydrates is technically feasible and has significant potential. Both depressurization and thermal stimulation seem to be capable of producing substantial amounts of CH_4 gas.

1. Introduction

Gas hydrates are solid compounds in which gas molecules are encaged inside the lattices of ice crystals. These gases are referred to as *guests*, whereas the ice crystals are called *hosts*. Of particular interest are hydrates in which the gas is a hydrocarbon. Under suitable conditions of low temperature and high pressure, hydrocarbon gases will react with water to form hydrates. The equation of formation or decomposition of hydrates from a hydrocarbon M and water is

$$M + nH_2O \rightleftharpoons M \cdot n_h\, H_2O,$$

where n_h is the hydration number.

Vast amounts of hydrocarbons are trapped in hydrate deposits [*Sloan*, 1998]. Such deposits exist where the thermodynamic conditions allow hydrate formation, and are concentrated in two distinctly different types of geologic formations where the necessary low temperatures and high pressures exist: in the permafrost and in deep ocean sediments. The lower depth limit of hydrate deposits is controlled by the geothermal gradient.

Current estimates of the worldwide quantity of hydrocarbon gas hydrates range between 10^{15} to 10^{18} m^3, and even the most conservative estimates of the total quantity of gas in hydrates may easily surpass by a factor of two the energy content of the total fuel fossil reserves recoverable by conventional methods [*Sloan*, 1998].

The majority of hydrocarbon gas hydrates are CH_4-hydrates. Such hydrates concentrate methane volumetrically by a factor of 164, and require less than 15% of the recovered energy for dissocation. CH_4-hydrates have a hydration number $n_h = 6$, and belong to the I crystalline structure [*Sloan*, 1991], which contains 46 H_2O molecules per unit cell. Depending on the thermodynamic state of the system, the amount of hydrate created or

released is determined from the equilibrium reactions

$$\begin{aligned} CH_4 \cdot 6H_2O &\rightleftharpoons CH_4(\text{gas}) + 6H_2O(\text{liquid}) \\ CH_4 \cdot 6H_2O &\rightleftharpoons CH_4(\text{gas}) + 6H_2O(\text{ice}). \end{aligned} \tag{1}$$

The magnitude of this resource makes methane hydrate reservoirs a substantial future energy resource. While current economic realities do not favor CH_4 production from hydrates, the potential of this resource clearly demands evaluation.

Three methods have been proposed for recovering CH_4 from hydrate deposits. The first method is thermal stimulation [*McGuire*, 1981], in which fluids at an elevated temperature are injected into the hydrate formation and effect CH_4 release by temperature The second method is depressurization [*Holder et al.*, 1982], in which the CH_4 release is achieved by lowering the pressure below that of the hydrate stability field at a given temperature. The third method is inhibitor injection [*Kamath and Godbole*, 1987], in which the CH_4 is produced after the injection of substances (e.g., brines, methanol, glycol) which destabilize the hydrate. Combinations of these methods can also be used.

In this paper, we present the development of EOSHYDR, a TOUGH2 [*Pruess*, 1991] module for the simulation of the potential of recovering gas from hydrate reservoirs. EOSHYDR is designed to model the non-isothermal CH_4 release, phase behavior and flow under the conditions of the common methane hydrate deposits (i.e., in the permafrost and in deep ocean sediments) by solving the coupled equations of mass and heat balance. Although CH_4-hydrates contain small amounts of other gaseous components, which are important for nucleation [*Sloan*, 1998], in this module we assume pure CH_4.

2. Governing Equations

A non-isothermal CH_4-hydrate system can be fully described by three mass balance equations and an energy balance equation. Following *Pruess* [1987; 1991], the components

$$\kappa \equiv \begin{cases} w & \text{for water} \\ m & \text{for } CH_4 \\ h & \text{for heat} \end{cases} \qquad \text{and} \qquad \kappa \equiv \begin{cases} w & \text{for water} \\ m & \text{for } CH_4 \text{ gas} \\ c & \text{for } CH_4\text{-hydrate} \\ h & \text{for heat} \end{cases}$$

under equilibrium and kinetic conditions, respectively, are considered. Mass balance in every subdomain (gridblock) n into which the flow domain is subdivided by the integral

finite difference method of TOUGH2 [*Pruess*, 1991] dictates that

$$\frac{d}{dt}\int_{V_n} M^\kappa \, dV = \int_{\Gamma_n} \mathbf{F}^\kappa \cdot \mathbf{n} \, d\Gamma + \int_{V_n} q^\kappa \, dV \, , \tag{2}$$

where

V, V_n volume, volume of subdomain n [m^3];

M^κ mass accumulation term of component κ [kg m^{-3}];

M^h energy accumulation term [J m^{-3}];

Γ_n surface area of subdomain n [m^2];

$\mathbf{F}^\kappa$ Darcy flux vector of component κ [kg m^{-2} s^{-1} or J m^{-2} s^{-1}];

$\mathbf{n}$ inward unit normal vector [*dimensionless*];

q^κ source/sink term of component κ [kg m^3 s^{-1} or J m^3 s^{-1}];

t time [s].

Under the conditions of production from a natural CH_4-hydrate formation (i.e., in the permafrost or in deep marine sediments) there are four possible phases β: an aqueous phase ($\beta \equiv w$), a gaseous phase consisting of water vapor and CH_4 ($\beta \equiv g$) , a *solid* phase composed of CH_4-hydrates ($\beta \equiv s$), and a *solid* ice phase ($\beta \equiv i$).

2.1. Accumulation Terms

EOSHYDR allows both equilibrium and kinetic hydrate formation or dissociation. Under equilibrium conditions, the mass accumulation terms M^κ in equation (2) are given by

$$\begin{aligned} M^w &= \sum_{\beta \equiv w,g,i} \phi \, S_\beta \, \rho_\beta \, X_\beta^w + k_1 \, \phi \, \rho_c \, P_g^m \\ M^m &= \sum_{\beta \equiv w,g,i} \phi \, S_\beta \, \rho_\beta \, X_\beta^m + k_2 \, \phi \, \rho_c \, P_g^m \, , \end{aligned} \tag{3}$$

where

ϕ porosity [*dimensionless*];

ρ_β density of phase β [kg m^{-3}];

S_β saturation of phase β [*dimensionless*];

X_β^κ mass fraction of component κ ($\equiv w, m, c$) in phase β [kg/kg]

P_g^m partial pressure of CH_4 in the gas phase [Pa].

The parameter k_2 [m^3 Pa^{-1}] is a *partition coefficient* distributing CH_4 between the gas phase and the hydrate phase. In that respect, CH_4 in the hydrate is considered sorbed CH_4 gas in a manner akin to linear sorption, and the amount is a linear function of the partial pressure of CH_4. The value of k_1 is determined from the equilibrium constant $K = K(T)$ of Equation (1), which is given by

$$\ln K = -\frac{\Delta G^0}{RT} \qquad \text{and/or} \qquad \frac{d\ln K}{dT} = \frac{\Delta H^0}{RT^2} \tag{4}$$

where

ΔG^0 standard Gibbs energy change of hydrate formation or dissociation [J/mole];

ΔH^0 hydrate latent heat of formation or dissociation [J/mole];

R universal gas constant [= 8.3145 J mol^{-1} K^{-1}].

The equilibrium in Equation (1) dictates that

$$K = \frac{\alpha_m (\alpha_w)^6}{\alpha_c}. \tag{5}$$

In Equation (5), α is the activity of the component denoted by the subscript, and the subscripts m, w and c denote CH_4, H_2O and CH_4-hydrate, respectively. For CH_4,

$$\alpha_m = \frac{f}{f_0} = \frac{y\,\Phi\,P_g}{y\,\Phi_0\,P_{g0}}, \tag{6}$$

where

f fugacity of CH_4 in the gas phase [Pa];

Φ fugacity coefficient [dimensionless];

y mol fraction of CH_4 in the gas phase;

0 subscript denoting standard pressure [= 101300 Pa].

The fugacity coefficient Φ is determined from

$$\ln\Phi = \frac{b}{b_M}(z-1) - \ln\left(z - \frac{b_M P_g}{RT}\right) - \frac{a_M}{b_M RT}\left[\frac{2\sum_i y_i a_{ij}}{a_M} - \frac{b}{b_M}\right]\ln\left(1 + \frac{b_M P}{zRT}\right), \tag{7}$$

in which the summation is over the components i in the gas phase. The compressibility $z = PV/RT$ and the terms a and b are obtained from the Soave-Redlich-Kwong equation of state [*Soave*, 1972], i.e.,

$$P = \frac{RT}{V-b} - \frac{a}{V(V-b)}, \tag{8}$$

$$z^3 - z^2 + (A - B - B^2)\, z - a\, B = 0, \tag{9}$$

where

$$a(T) = a_c(T_c)\, \gamma(T_r, \omega), \tag{10}$$

$$a_c(T_c) = 0.42747\ R^2\, T_c^2/P_c\,, \qquad \gamma(T_r, \omega) = \left[1 + \eta(1 - T_r)^{0.5}\right]^2 \tag{11}$$

$$\eta = 0.48508 + 1.55171\omega - 0.15613\omega^2\,, \qquad b = 0.08664\, R\, T_c/P_c\,, \tag{12}$$

with

$$A = \frac{a\, P}{(RT)^2} \qquad \text{and} \qquad B = \frac{b\, P}{RT}\,. \tag{13}$$

The variables T_c, P_c and ω are the critical temperature, critical pressure, and the accentric factor of the gaseous component, respectively, while T_r is the reduced temperature defined as $T_r = T/T_c$. The subscript M in (7) denotes the miing parameters, which are defined as

$$a_M = \sum_i \sum_j y_i\, y_j\, a_{ij}, \quad b_m = \sum_i y_i\, b_i, \quad a_{ij} = (a_i\, a_j)^{1/2}(1 - k_{ij}), \tag{14}$$

where $a_{12} = a_{21}$. The interaction parameters k_{ij} are close to zero for interactions between hydrocarbons, but are significantly different from zero for hydrocarbon-water interactions [*Sloan*, 1998].

The activity of the hydrate α_c in Equation (5) is essentially constant at a given temperature regardless of wherher the other phase is present. The activity α_w is taken to be equal to one at relatively low pressures because of the low solubility of methane in water. In the presence of an inhibitor (such as salt in the water in ocean sediments of hydrates), α_w is determined from Pieroen's equation [*Sloan*, 1998]

$$\ln\alpha_w = \frac{\Delta H^0}{6\, R}\left[\frac{1}{T_w} - \frac{1}{T_s}\right], \tag{15}$$

where T_w and T_s are the hydrate formation temperatures [K] in pure water and in the salt solution, respectively. The hydrate formation temperature in the presence of salt, T_s, is obtained from the equation [*Sloan*, 1998]

$$T_s = \left[\frac{1}{T_w} - \frac{3.6046 \times 10^4}{\Delta H^0}\left(\frac{1}{273.15} - \frac{1}{T_{fs}}\right)\right]^{-1}, \tag{16}$$

where T_{fs} is the freezing point of the salt solution [K].

The parameter k_1 in equation (3) is related to k_2 through the stoichiometry of the hydrate. It is obvious that

$$\frac{k_1}{k_2} = \frac{6\,W^w}{W^m} = 6.75, \tag{17}$$

where W^w and W^m are the molecular weights [kg mol^{-1}] of water and CH_4, respectively. The amount of water released from the hydrates is added either to the aqueous or the ice phase, according to the prevailing thermodynamic conditions.

The heat of dissociation ΔH^0 in equation (4) under three-phase conditions (L_w-H-V or I-H-V) is determined from the Clausius-Clapeyron equation

$$\Delta H^0 = z\,R\,T^2 \frac{d\ln P}{dT}, \tag{18}$$

which is in excellent agreement with experimental data [*Sloan*, 1998]. The heat of hydrate formation under three-phase conditions is given by the equation

$$\Delta H^0 = C_1(T) + \frac{C_2(T)}{T}, \tag{19}$$

where C_1 and C_2 are experimental parameters (functions of T) determined by *Kamath* [1984].

The values of some mass fractions can be determined *a priori*. Assuming that the solubility of the CH_4 gas in ice is sufficiently small to be considered negligible, $X_i^m = 0$ and $X_i^w = 1$. From the stoichiometry of hydrates, $X_s^w = 0.87097$ and $X_s^m = 0.12903$.

Kinetic data on hydrate formation and dissociation under conditions characteristic of their presence in the subsurface are not available [*Sloan*, 1998]. Kinetic data from laboratory studies [*Englezos et al.*, 1987*a*,*b*; *Skovborg and Rasmussen*, 1994; *Kamath*, 1984; *Selim and Sloan*, 1985] appear to be specific to the apparatus used in the study, involve parameters

which are difficult to evaluate, and have limited applicability to reservoir-level studies. EOSHYDR allows consideration of kinetic hydrate formation or dissolution assuming a standard kinetic model, with parameters which may become available in the future from appropriate laboratory experiments.

Under kinetic conditions, the mass accumulation terms M^κ in Equation (2) are given by

$$M^\kappa = \sum_{\beta \equiv w,g,s,i} \phi\, S_\beta\, \rho_\beta\, X_\beta^\kappa, \qquad \kappa \equiv w,m,c\,. \tag{20}$$

In the kinetic model,

$$\begin{aligned} &\text{for} \quad \beta \equiv w : X_w^c = 0, \\ &\text{for} \quad \beta \equiv g : X_g^c = 0, \\ &\text{for} \quad \beta \equiv s : X_s^w = X_s^m = 0, \quad X_s^c = 1, \quad \text{and} \\ &\text{for} \quad \beta \equiv i : X_i^m = X_i^c = 0, \quad X_i^w = 1. \end{aligned}$$

The heat accumulation term includes contributions from the rock matrix and all the phases, and is given in both the equilibrium and the kinetic model by the equation

$$M^h = (1-\phi)\,\rho_R\, C_R\, T + \sum_{\beta \equiv w,g,s,i} \phi\, S_\beta\, \rho_\beta\, u_\beta \tag{21}$$

where

ρ_R rock density [kg m^{-3}];

C_R heat capacity of the dry rock [J kg^{-1} K^{-1}];

T temperature [K];

u_β specific internal energy of phase β.

Due to the limited solubility of CH_4 in the aqueous phase under the conditions of CH_4-hydate occurence in the subsurface, a good approximation to u_w is obtained by the aqueous phase to be pure water. The specific internal energy of the gaseous phase is a very strong function of composition, and is given by

$$u_g = \sum_{\kappa \equiv w,m} X_g^\kappa\, u_g^\kappa\,, \tag{22}$$

where u_g^κ is the specific internal energy of component κ in the gaseous phase.

2.2. Flux Terms

The mass fluxes of water and CH_4 gas include contributions from the aqueous and gaseous phases, i.e.,

$$\mathbf{F}^\kappa = \sum_{\beta \equiv w,g} \mathbf{F}_\beta^\kappa, \qquad \kappa \equiv w, m. \tag{23}$$

The contributions of the two solid phases ($\beta \equiv s, i$) to the fluid fluxes are zero. Therefore, in the kinetic model the mass flux of the hydrate component ($\kappa \equiv c$) across all subdomain boundaries is

$$\mathbf{F}^c = 0. \tag{24}$$

For the aqueous phase, $\mathbf{F}_w^w = X_w^w \mathbf{F}_w$, and the phase flux $\mathbf{F}_w$ is described by Darcy's law

$$\mathbf{F}_w = -k \frac{k_{rw}\, \rho_w}{\mu_w} \left(\nabla P_w - \rho_w \mathbf{g}\right), \tag{25}$$

where

k rock intrinsic permeability [m^2];

k_{rw} relative permeability of the aqueous phase [$dimensionless$];

μ_β viscosity of the aqueous phase [Pa s];

P_w pressure of the aqueous phase [Pa];

$\mathbf{g}$ gravitational acceleration vector [ms^{-2}].

The aqueous pressure P_w is given by

$$P_w = P_g + P_{cgw}, \tag{26}$$

where $P_g = P_g^m + P_g^w$ is the gas pressure [Pa],P_{cgw} is the gas-water capillary pressure [Pa], and P_g^m, P_g^w are the CH_4 gas and water vapor partial pressures [Pa], respectively. The solubility of CH_4 in the aqueous phase is related to P_g^m through Henry's law,

$$P_g^m = H^m X_w^m \frac{W^w}{W^m}, \tag{27}$$

where $H^m = H^m(P_g, T)$ is a factor akin to Henry's constant. H^m values for both fresh water and seawater were obtained from *Vargaftik* [1975] and *Handa* [1990].

The mass flux of the gaseous phase ($\beta \equiv g$) incorporates advection and diffusion contributions, and is given by

$$\mathbf{F}_g^\kappa = -k_0 \left(1 + \frac{b}{P_g}\right) \frac{k_{rg}\,\rho_g}{\mu_g} X_g^\kappa \left(\nabla P_g - \rho_g\,\mathbf{g}\right) + \mathbf{J}_g^\kappa, \quad \kappa \equiv w, m, \tag{28}$$

where

k_0 absolute permeability at large gas pressures (= k) [m^2];

b *Klinkenberg* [1941] b-factor accounting for gas slippage effects [Pa];

k_{rg} relative permeability of the gaseous phase [*dimensionless*];

μ_β viscosity of the gaseous phase [Pa s].

The term $\mathbf{J}_g^\kappa$ is the diffusive mass flux of component κ in the gas phase [kg m^{-2} s^{-1}], and is described by

$$\mathbf{J}_g^\kappa = -\phi\, S_g \underbrace{\left(\phi^{1/3} S_g^{7/3}\right)}_{\tau_g} D_g^\kappa\, \rho_g\, \nabla X_g^\kappa, \qquad \kappa \equiv w, m, \tag{29}$$

where D_g^k is the multicomponent molecular diffusion coefficient of component κ in the gas phase in the absence of a porous medium [m^2 s^{-1}], and τ_g is the gas tortuosity [*dimensionless*] computed from the *Millington and Quirk* [1961] model. The diffusive mass fluxes of the water vapor and CH_4 gas are related through the relationship of *Bird et al.* [1960]

$$\mathbf{J}_g^w + \mathbf{J}_g^m = 0, \tag{30}$$

which ensures that the total diffusive mass flux of the gas phase is zero with respect to the mass average velocity when summed over the two components ($\kappa \equiv w, m$) . Then the total gas phase mass flux is the product of the gas phase Darcy velocity and the gas phase density.

The heat flux accounts for both conduction and convection, and is given by

$$\begin{aligned} \mathbf{F}^h = &- \left\{(1-\phi)\, K_R \; + \phi\left[S_s\, K_s + S_i\, K_i + S_w\, K_w + S_g\, K_g\right]\right\} \nabla T \\ &+ \sum_{\beta \equiv w, m} h_\beta\, \mathbf{F}_\beta, \end{aligned} \tag{31}$$

where

K_R thermal conductivity of the rock [W m^{-1} K^{-1}];

K_β thermal conductivity of phase $\beta \equiv w, g, s$ [W m^{-1} K^{-1}];

h_β specific enthalpy of phase $\beta \equiv w, g, s$ [J kg^{-1}].

For the reasons discussed in Section 2.1, the aqueous phase specific enthalpy is assumed to be that of pure water, and the gas phase specific enthalpy is computed as

$$h_g = \sum_{\kappa \equiv w, m} X_g^\kappa \, h_g^\kappa, \tag{32}$$

where $h_g^\kappa, \kappa \equiv w, m$ is the specific enthalpy of the water vapor and CH_4 gas, respectively. The relationship between enthalpy h and internal energy u is described by the thermodynamic equation

$$h = u + \frac{P}{\rho}, \tag{33}$$

where ρ is the density of the gas.

2.3. Source and Sink Terms

In the equilibrium model, injection of a fluid into the reservoir can occur at mass rates $\hat{q}^\kappa, \kappa \equiv w, m$, while removal of the compounds is described by

$$\hat{q}^\kappa = \sum_{\beta = w, g} X_\beta^\kappa \, q_\beta, \qquad \kappa \equiv w, m, \tag{34}$$

where q_β is the production rate of the phase β.

In the kinetic model, the additional sink/source terms corresponding to hydrate dissociation and release of CH_4 and H_2O must be accounted for. The source term for CH_4 thus becomes $\hat{q}^m + Q^m$, where the production rate Q^m [kg m^{-3} s^{-1}] of CH_4 is taken from reaction kinetics as

$$Q^m = k^m \, W^m \, [CH_4]^\theta = k^m \, W^m \left(\frac{P_g^m}{RTz} \right)^\theta, \tag{35}$$

where

k^m $= k_m(T)$, reaction constant [m$^{3\theta}$ mol$^{1-\theta}$ s^{-1}];

$[CH_4]$ molar concentration of CH_4 [mol m^{-3}];

θ order of the reaction [dimensionless].

The fact that the dissociation of CH_4-hydrates involves a CH_4 gas and, depending on the thermodynamic conditions, either two solid phases or a solid and a liquid phase (hydrate and ice), provides supporting evidence that Equation (35) describes representatively the rate of CH_4 release. Although currently there is no information on k_m and θ, EOSHYDR includes this model because of the importance of kinetic behavior of CH_4-hydrates.

The source term for water (aqueous or ice phase) is $q^w + Q^w$, where the hydrate-related release of water Q^w is determined from the stoichiometry of Equation (1) as

$$Q^w = \frac{6W^w}{W^m} Q^m . \tag{36}$$

Similarly, the sink term corresponding to the hydrate compound is

$$\hat{q}^c = Q^c = -\frac{W^c}{W^m} Q^m , \tag{37}$$

where W_c is the molecular weight of the CH_4-hydrate.

Under equilibrium conditions, the rate of heat removal or addition includes contributions of (a) the heat associated with fluid removal or addition, as well as (b) direct heat inputs or withdrawals (e.g., microwave heating), and is described by

$$\hat{q}^h = q_d + \sum_{\beta = w, g} h_\beta \, q_\beta . \tag{38}$$

Under kinetic conditions, Equation (38) is extended to account for the heat of dissociation, thus becoming

$$\hat{q}^h = q_d + \sum_{\beta = w, g} h_\beta \, q_\beta + \hat{q}^c \, \Delta H^0 . \tag{39}$$

2.4. Primary Variables

In order to describe the thermodynamic state of the three- or four-component system (two mass components and a heat component under equilibrium conditions, three mass components and a heat component under kinetic conditions) in EOSHYDR, a set of three or four appropriate *primary* variables must be selected. All other *secondary* parameters (which

include thermodynamic and transport properties of the system) needed for the solution of the four coupled equations in Equation (1) are computed from the primary variables.

Under equilibrium conditions, the three primary variables in EOSHYDR are (a) the gas pressure P_g, (b) the saturation of the gas phase S_g, and (c) the temperature T. Under kinetic conditions, the four primary variables in EOSHYDR are (a) the gas pressure P_g, (b) the saturation of the gas phase S_g, (c) the CH_4-hydrate saturation S_s, and (d) the temperature T. This selection of variables allows simulations when the aqueous phase is absent.

The computation of the secondary variables (i.e., aqueous phase density, gas phase density and mass fractions, gas phase viscosity, capillary pressures, relative permeabilities, diffusivities for water and CH_4) follows the approach in the TOUGH2 [*Pruess*, 1991] and T2VOC [*Falta et al.*, 1995]. In the computation of saturation-dependent properties (i.e., capillary pressure and relative permeabilities of the gas and aqueous phases), the properties of the porous medium free of hydrates are used.

2.5. Phase Equilibrium

The phases discussed in this section should not be confused with the phases considered in the formulation of the mass and heat balance equations, but are rather the thermodynamic phases in the P-T-X diagram of CH_4 and H_2O. Thermophysical properties in EOSHYDR are obtained from the Pressure-Temperature-Composition (P-T-X) diagram of CH_4 [*Kobayashi and Katz*, 1949], as well as from CH_4 property tables [*Vargaftik*, 1975] and the water tables available in TOUGH2 [*Pruess*, 1991]. The water tables in TOUGH2 were extended to cover the -50 C to 500 C range.

The phases in the P-T-X diagram are: V (vapor), L_w (liquid water), I (ice), H (hydrate), M (solidified methane), and L_m (liquid methane). Of particular interest are the pressures and tempereatures of the L_w-H-V and I-H-V three-phase lines, which delineate the limits to hydrate formation. The relationship between the three-phase P and T in EOSHYDR is obtained from a regression fit [*Kamath*, 1984] to a set of experimental data listed in *Sloan* [1998], which yielded the equation

$$P = \exp\left(e_1 + \frac{e_2}{T}\right), \tag{40}$$

where P is in Kpa, T is in K,

$$e_1 = \begin{cases} 38.980 \\ 14.717 \end{cases} \quad \text{and} \quad e_2 = \begin{cases} \text{-8533.80} & \text{for } 0^oC \geq T \geq 25^oC \\ \text{-1886.79} & \text{for } -25^oC \geq T \geq 0^oC. \end{cases} \tag{41}$$

Hydrates may also exist in equilibrium with CH_4 when there is no aqueous phase present, in which case the two possible two-phase systems are H-V and H-L_m. In the three-phase regions, only one intensive variable is needed to specify a binary system; however, two variables are needed to specify the two-phase binary system [*Sloan*, 1998]. Typically, the water concentration at a specified pressure and temperature is determined as the second variable using the algorithm of *Sloan* [1998].

3. Test Problems

3.1. Test Problem 1

Test Problem 1 involves the depressurization-induced release of CH_4 in a reservoir containing stratified layers of CH_4 gas and hydrate deposits under permafrost conditions. Figure 1 and Table 1 show a schematic of the reservoir and the reservoir properties, respectively. Gas is produced in a single well completed throughout the gas zone. The well is located at the center of the reservoir, and its production rate is constant at 0.81944 $m^3\ s^{-1}$ (2.5 MMFCD).

The problem was first studied by *Holder et al.* [1982], who solved the uncoupled pressure and temperature equations by using a 2-D grid for pressure calculations and a 3-D grid for temperature calculations. In their approach, the heat transferred to the interface (due to the temperature gradient) was used for the hydrate dissociation, and there was no energy balance based on the existing phases and their enthalpies.

Because of the radial symmetry of the problem and the need to have a higher definition in the vicinity of the well bore, we used a 2-D cylindrical system to simulate the reservoir. The reservoir radius was $r = 567.5$ m, and its thickness was $Z = 30.5$ m (100 ft) equally distributed between the hydrate layer and the free gas zone. These dimensions result in a reservoir with a volume identical to the cartesian system of *Holder et al.* [1982].

The system was discretized in $(80 \times 40 = 3200)$ gridblocks in (r, z). Using the equilibrium model, a total of 9600 coupled equations were solved simultaneously. The 40

Δz dimensions were (moving from the reservoir top down) were 1.5 m, 12×1 m, 0.5 m, 0.3 m, 2×0.2 m, 6×0.1 m, 0.3 m, 2×0.2 m, 0.3 m, 0.5 m, 12×1 m and 1.5 m. The Δr dimensions were 0.1 m (the wellbore radius), 0.1 m, 0.2 m, 0.3 m, 0.5 m, and the remaining 75 Δr were determined from a logarithmic distribution, in which the first Δr = 0.5 m, and the multiplier is determined from the requirement that the outer radius be equal to 567.5 m. This discretization provided substantial detail near the wellbore. The wellbore itself was simulated by the first column of gridblocks at the origin of the system, in which the vertical permeability had been set to 1 m^2, i.e., practically infinite compared to the reservoir permeability of 4.3425×10^{-14} m^2 (44 md). The horizontal permeability of the wellbore gridblocks was zero in the hydrate layer and equal to the reservoir permeability in the free gas zone. The production rate was assigned to the top wellbore gridblock.

Two cases were tested. In the Case 1, the initial hydrate saturation in the hydrate zone was $S_s = 1$, which results in zero initial fluid permeability in this region. However, after the beginning of dissociation, the permeability of gas and released water are no longer zero, and they are determined by the relative permeability curve and the gas and aqueous saturation (S_g and S_w) in the hydrate zone. In Case 2, $S_g = 0.7$ and $S_w = 0.3$.

For the relative permeability and capillary pressure curves, the *van Genuchten* [1980] model (available in TOUGH2) was used, according to which

$$\begin{aligned} k_{rw} &= \overline{S}_w^{1/2} \left[1 - \left(1 - \overline{S}_w^{1/m}\right)^m\right]^2 \\ k_{rg} &= \overline{S}_g^{1/2} \left(1 - \overline{S}_w^{1/m}\right)^{2m} \\ P_c &= -C_p \left[(\overline{S}_w)^{-1/m} - 1\right]^{1-m}, \end{aligned} \tag{42}$$

where

$$\overline{S}_w = \frac{S_w - S_r}{1 - S_r}, \qquad \overline{S}_a = \frac{S_a - S_r}{1 - S_r}, \tag{43}$$

and S_r is the irreducible water saturation. In hydrate reservoirs, the sum $\overline{S}_w + \overline{S}_g \neq 1$ because of the presence of the hydrate and the ice phases. In this simulation, $S_r = 0.1$, $m = 0.45$ and $C_p = 10^5$ Pa.

Figure 2 shows the cumulative contribution of hydrate dissociation to the total gas production as a function of production times. Compared to the *Holder et al.* [1982] results,

our simulation indicates a much higher contribution of dissociated gas in Case 1 (which corresponds to the *Holder et al.* [1982] conditions). The difference is attributed to the fact that in our model a gas phase emerges in the hydrate zone, which keeps expanding as the dissociation continues and the released water drains. Additionally, the water released through decomposition occupies a volume 13% smaller than the corresponding hydrate, thus further increasing S_g. In Case 2, the cumulative contribution of dissociated gas is higher due to the higher permeability to gas movement.

Figure 3 shows the vertical temperature profiles at a distance $r = 0.15$ m from the wellbore. In Case 1, the maximum temperature decrease is 8.23 K, occurs at $z = -14.6$ m, i.e., 0.4 m above the initial interface, and is significantly larger than the 1.2 K drop reported by *Holder et al.* [1982]. We believe that the differences are due to the reasons mentioned above, as well as to the much finer discretization in the vicinity of the well bore. In case 2, the maximum temperature decrease is 7.11 K and occurs 0.6 m above the initial interface. The differences between cases 1 and 2 are attributed to the higher gas permeability in Case 2.

Figure 4 shows the evolution over time of the pressure at the wellbore gridblock immediately below the initial interface (at $r = 0.05$ m and $z = -15.05$ m). The pressure in Case 1 is lower than the *Holder et al.* [1982] results, but the difference is rather small. It appears that the reason for the similarity of the answers is that the finer discretization and higher dissociation in our model produce roughly the same results as the coarser discretization and lower dissociation of the *Holder et al.* [1982] model. The pressures in Case 2 are larger than those in Case 1 due to the higher permeability (and, consequently, the higher hydrate dissociation) of the gas phase.

3.2. Test Problem 2

Test Problem 2 involves the depressurization-induced release of CH_4 in a reservoir of CH_4 hydrates and salt water (no free gas phase), i.e., under conditions of ocean sediments. The distribution of water and hydrate was uniform throughout the reservoir, with initial $S_w = S_s = 0.5$ and $S_g = 0$. The reservoir dimensions, properties, and the initial conditions were the same as in Problem 1. The properties of fresh water were used in this simulation, but the effect of salt on the hydrate dissociation as accounted for. Fluids were produced by

setting the pressure at the wellbore gridblock at $z = -14.95$ m, i.e., immediately above the interface, constant at 1.7237×10^7 Pa (2500 psi), and were distributed in the production stream according to their mobilities.

The cumulative gas production over time (shown in Figure 6) is roughly proportional to the square root of time, and reaches the level of 4.114×10^7 m^3 (1.453×10^9 ft^3) after a year of production. The reason for this high level of production appears to be the very high compressibility of water. The temperature distribution along z at $r = 0.15$ m (Figure 7) tends to support this thesis, as the temperature decrease is larger and more extended than in Problem 1. Although this is a simplified example, the results are encouraging for CH_4 production from hydrates in ocean sediments.

3.3. Test Problem 3

Test Problem 3 simulates the release of CH_4 through a thermal stimulation process in a reservoir of CH_4 hydrates and free CH_4 gas phase, i.e., under permafrost conditions. The problem simulated here is the frontal sweep production system discussed by *McGuire* [1981], which is similar to the steam flooding process in heavy-oil reservoirs. The frontal sweep method involves wells arranged in a *five-spot* pattern (Figure 8). The injected fluid was hot water because the parametric study of *McGuire* [1981] indicated that when steam is injected steam, the amount of produced gas was less than the estimated fuel consumption.

Because of symmetry, only 1/4 of the basic pattern needs to be modeled. The side of the basic square was 500 m, and the thickness of the reservoir was 30.5 m (100 ft). The domain was discretized in $20 \times 20 \times 20 = 8000$ gridblocks in (x, y, z), resulting in a uniform gridblock size of 25 m$\times$25 m$\times$1.525 m and a total of 24000 equations (equilibrium model). The injection well was completed in the bottom half of the reservoir, while the production well was completed in the top half. The reservoir porosity was 0.25, and initially $S_s = 0.6$ and $S_w = 0.4$. All other reservoir properties and the initial pressure and temperature were the same as in the Test Problem 1. It was not possible to simulate the problem as described by *McGuire* [1981] because in his approach the porous medium and its effects on flow were neglected.

Water at 333.15 K was injected at a rate of 0.055 kg s^{-1} at the injection well. This injection rate is the same with the one used in the *McGuire* [1981] study. Figure 9 shows

the cumulative CH_4 production over a year of injection and gas production. At the end of the year, the amount of produced CH_4 (2.36×10^7 m^3) is substantially smaller than the *McGuire* [1981] estimate (4.96×10^7 m^3) for the same injection temperature. This was expected because the *McGuire* [1981] model was not a porous medium model and did not take into account the resistance to flow that the hydrates present [*Holder et al.*, 1984]. Thus, the *McGuire* [1981] predictions were highly optimistic. The produced gas, however, is well above the (1.41×10^7 m^3) level necessary to cover the fuel consumption for heating the injected water

Figure 10 shows the temperature distribution along the line connecting the producing and injection well at $z = -16$ m from the reservoir top at $t = 1$ year. The curve exhibits a regions of temperature decline associated with the advancing hot water front. A second region with declining temperatures below the initial temperature level is evident in the vicinity of the production well, and is attributed to the inevitable depressurization process as fluids are withdrawn.

4. Summary and Discussion

We developed EOSHYDR, a new module for the TOUGH2 general-purpose simulator for three-dimensional, multi-component, multiphase fluid and heat flow and transport in the subsurface. EOSHYDR is designed to model the non-isothermal CH_4 release, phase behavior and flow under the conditions of the common methane hydrate deposits (i.e., in the permafrost and in deep ocean sediments) by solving the coupled equations of mass and heat balance. As with all other members of the TOUGH2 family of codes, EOSHYDR can handle multi-dimensional flow domains and cartesian, cylindrical or irregular grids, as well as porous and fractured media.

In EOSHYDR both an equilibrium and a kinetic model of hydrate formation or dissociation are included. Two new solid phases are introduced, one for the CH_4-hydrate and the other for ice. Under equilibrium conditions, water and methane, as well as heat, are the main components. In the kinetic model, the solid hydrate is introduced as the fourth component. The mass components are partitioned among the gas, liquid and the two solid phases. The thermodynamic phase equilibrium in EOSHYDR is described by the P-T-X

diagram of the H_2O - CH_4 system. Phase changes and the corresponding heat transfers are fully described. The effect of salt in pore waters on CH_4 solubility and on the growth and decomposition of gas hydrates is also taken into account. The current model does not account for the effects of dilution of the salty water on hydrate inhibition and dissociation (a potentially important issue in the injection of hot brines for inhibitor-induced dissociation), but this could be accomplished rather easily by the addition the salt mass balance equation.

Although EOSHYDR has the ability to model kinetically-controlled hydrate dissociation, only the equilibrium model was used in the three tests conducted in this study because of lack of the necessary parameters. The first test involved CH_4 production from a stratified reservoir of CH_4-hydrate and free CH_4 gas through a depressurization process under permafrost conditions with zero and non-zero initial gas saturation in the hydrate zone. The second test modeled depressurizatin-induced CH_4 production from a reservoir of CH_4-hydrate and salt water (uniformly distributed) under oceanic conditions. The third test modeled the thermal stimulation process of the frontal sweep system, which involved injection of hot water to dissocate CH_4 in a CH_4-hydrate and water reservoir.

The results of the tests tend to indicate that CH_4 production from CH_4-hydrates is technically feasible and has significant potential. Both depressurization and thermal stimulation seem to be capable of producing substantial amounts of CH_4 gas. Although the depressurization method appears to have an advantage over the thermal stimulation process, it is not possible to render a definitive judgement because of the dearth of information on the properties of hydrate reservoirs and their thermodynamic behavior. There are practically no reliable measurements of the permeability, porosity and saturation of natural hydrate deposits, while the understanding of the kinetic behavior of hydrates is at a very early stage of advancement [*Sloan*, 1998]. The enormity and potential of this resource clearly demands evaluation, and numerical studies are a powerful and efficient way to accomplish this. While the current data on hydrates allow the determination of the model sensitivity to inputs and the relative importance of the various reservoir and production parameters, data representative of reservoir conditions must be obtained to render models sufficiently robust for practical applications.

Acknowledgments. This work was supported by the Laboratory Directed Research

and Development Program of Lawrence Berkeley National Laboratory under the U.S. Department of Energy, Contract No. DE-AC03-76SF00098. Drs. Stefan Finsterle and Curt Oldenburg are thanked for their insightful review comments.

References

Bird, R., W. E. Stewart, and E. N. Lightfoot, *Transport Phenomena*, John Wiley and Sons, New York, NY, 1960.

Englezos, P., N. Kalogerakis, P. D. Dholabhai, and P. R. Bishnoi, *Chem. Eng. Sci.*, **42(11)**, 2647, 1987a.

Englezos, P., N. Kalogerakis, P. D. Dholabhai, and P. R. Bishnoi, *Chem. Eng. Sci.*, **42(11)**, 2659, 1987a.

Falta, R. W., K. Pruess, S. Finsterle, and A. Batistelli, T2VOC User's Guide, *Report LBL-36400*, Lawrence Berkeley Laboratory, Berkeley, CA, 1980.

Handa, Y. P., *J. Phys. Chem.*, **94**, 2652, 1990.

Holder, G. D., P. F. Angert, V. T. John, and S. L. Yen, Simulation of gas production from a reservoir containing both gas hydrates and free natural gas, *Proc. Soc. Petr. Eng. Meet., New Orleans, LA, Sept. 26-29*SPE 11105, 1982.

Holder, G. D., V. A. Kamath, and S. P. Godbole, *Ann. Rev. Energy,* **9**, 427, 1984.

Holder, G. D., V. A. Kamath, and S. P. Godbole, *Ann. Rev. Energy,* **9**, 427, 1984.

Kamath, V. A., Study of heat transfer characteristics during dissociation of gas hydrates in porous media, Ph.D. dissertation, Univ. of Pittsburgh., Pittsburgh, PA, 1984.

Kamath, V. A., and S. P. Godbole, *J. Pet. Tech.*, **39**, 1379, 1987.

Klinkenberg, L. J., The permeability of porous media to liquids and gases, in *API Drilling and Production Practice* , New York, 1941.

Kobayashi, R., and D. L. Katz, *Trans. AIME,* **186**, 66, 1949.

McGuire, P. L., Methane hydrate gas production: An assessment of conventional production technology as applied to hydrate recovery, *Report LA-9102-MS*, Los Alamos National Laboratory, Los Alamos, NM, 1981.

Millington, R. J., and J. P. Quirk, *Trans. Faraday Soc.*, **57**, 1200, 1961.

Pruess, K., TOUGH User's Guide, *Report LBL-20700*, Lawrence Berkeley Laboratory,

Berkeley, CA, 1987.

Pruess, K., TOUGH2 - A general purpose numerical simulator for multiphase fluid and heat flow, *Report LBL-29400*, Lawrence Berkeley Laboratory, Berkeley, CA, 1991.

Selim, M. S., and E. D. Sloan, Modeling and dissociation of an in-situ hydrate, *Proc. 1985 California Reg. Meet. Soc. Petr. Eng., San Diego, CA, March 27-29*SPE 13597, 1997.

Skovborg, P., and P. Rasmussen, *Chem. Eng. Sci.*, **49**, 1131, 1994.

Sloan, E. D., *AIChE J.*, **37**, 1281, 1991.

Sloan, E. D., *Clathrate Hydrates of Natural Gases*, Marcel Dekker, Inc., New York, NY, 1998.

Soave, G., *Chem. Eng. Sci.*, **27**, 1197, 1972.

van Genuchten, M. D., *Soil Sci. Soc. Am. J.*, **44**, 892, 1980.

Vargaftik, N. B., *Tables on the Thermophysical Properties of Liquids and Gases*, John Wiley and Sons, New York, NY, 1975.

Table 1. Reservoir characteristics and properties	
Parameter	**Value**
Gas zone thickness	50 m
Hydrate zone thickness	50 m
Initial pressure P_0	2.07×10^7 Pa
Initial temperature T_0	293.43 K
Gas composition	100% CH_4
Permeability k	4.3425×10^{-14} m^2
Gas production rate $\hat{q}_m$	0.82 m^3 s^{-1}
Thermal conductivity	1.5 W m^{-1} K^{-1}
Thermal diffusivity	7×10^{-7} m^2 s^{-1}

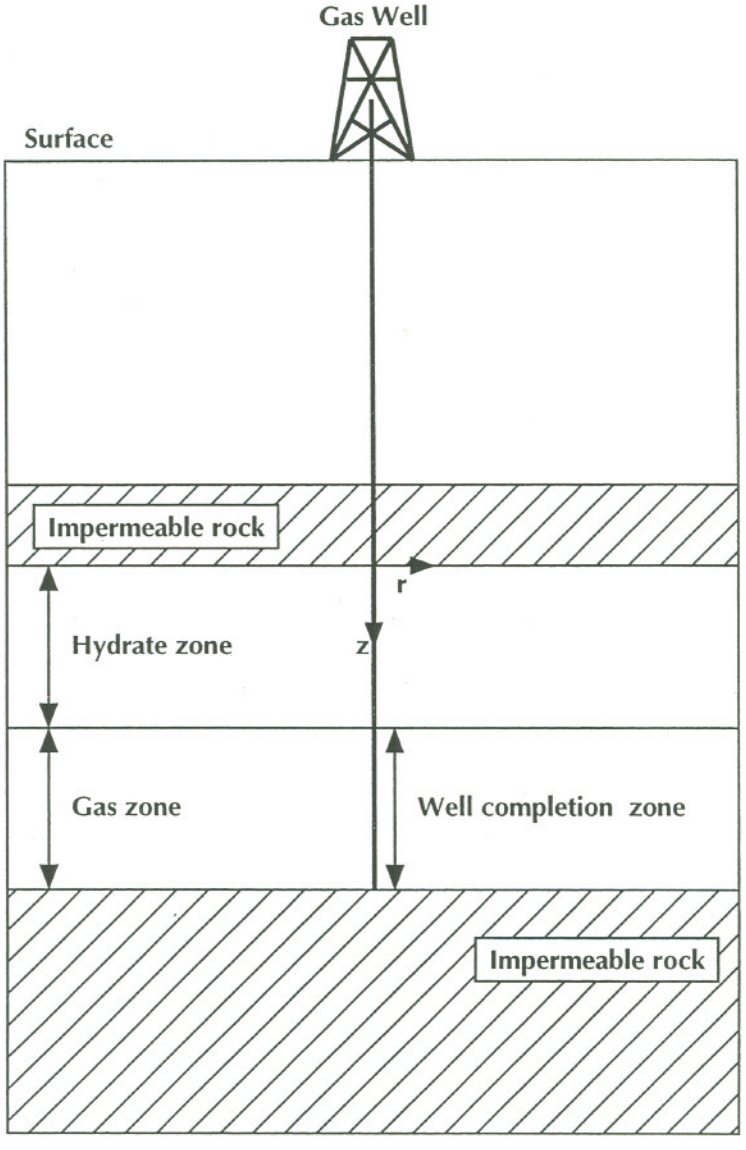

Figure 1. The reservoir configuration in Test Problem 1.

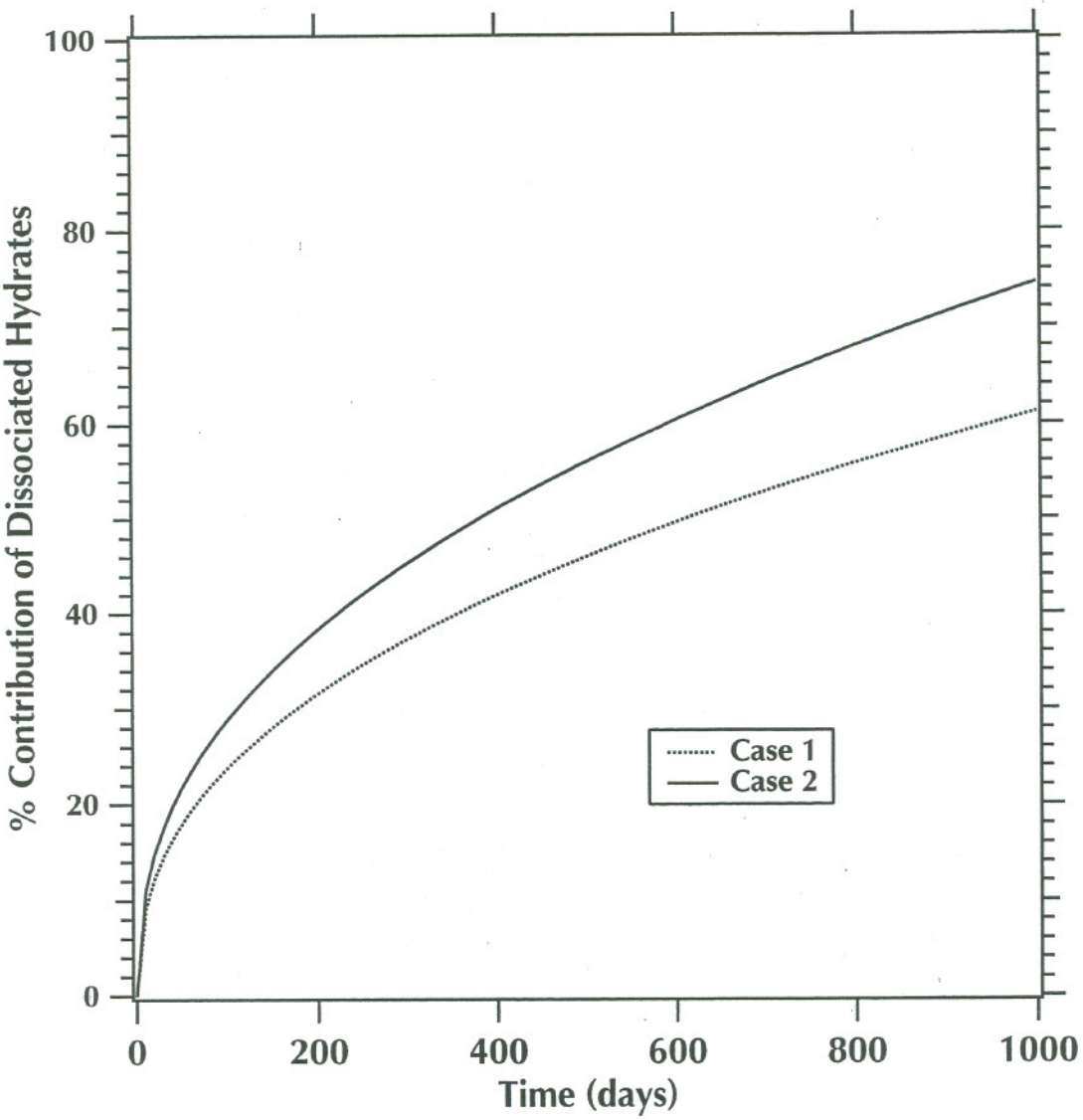

Figure 2. Cumulative contribution of CH_4 dissociated from hydrates to the total gas production in Test Problem 1.

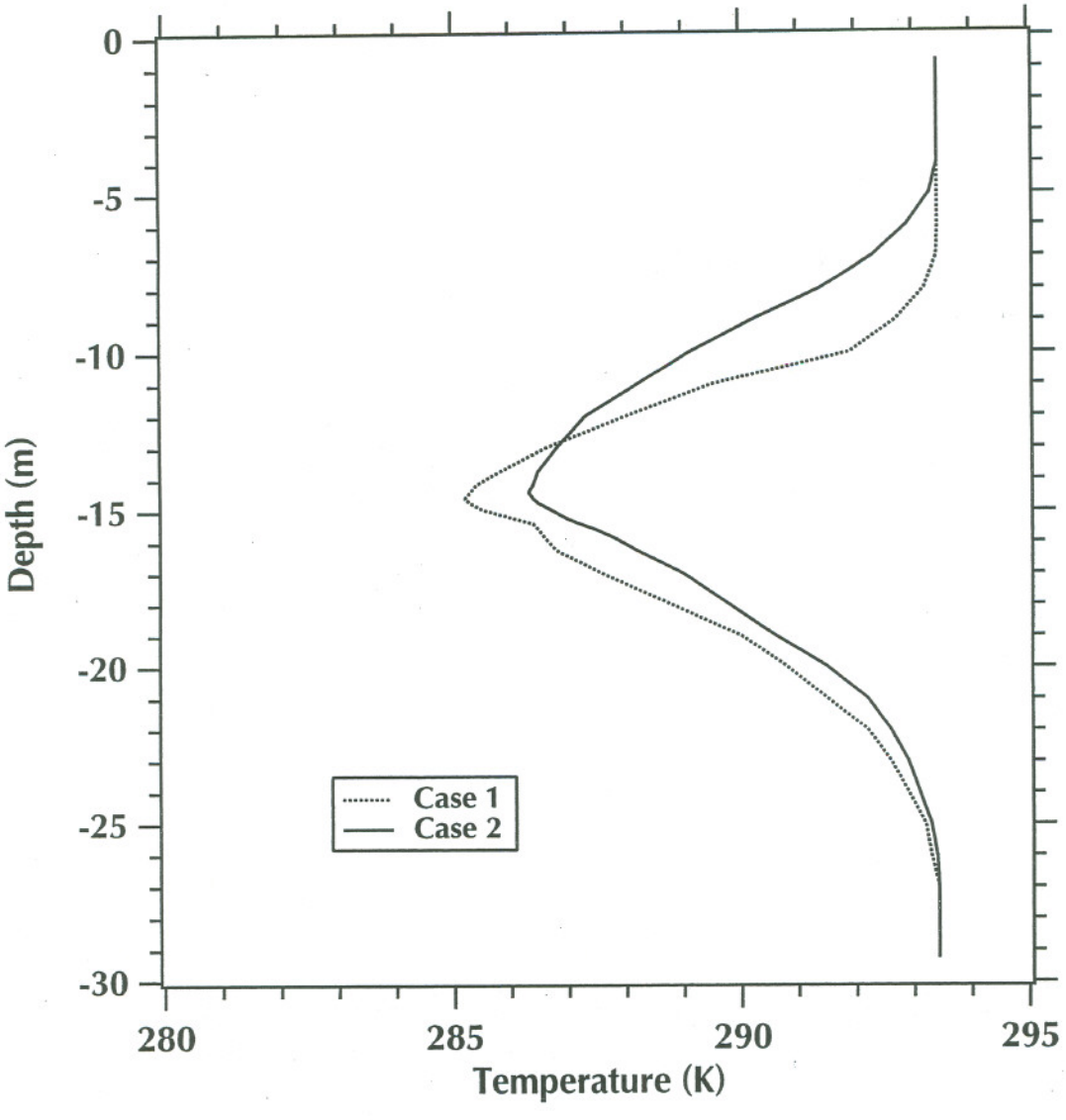

Figure 3. Vertical temperature distribution at $r = 0.15m$ in Test Problem 1.

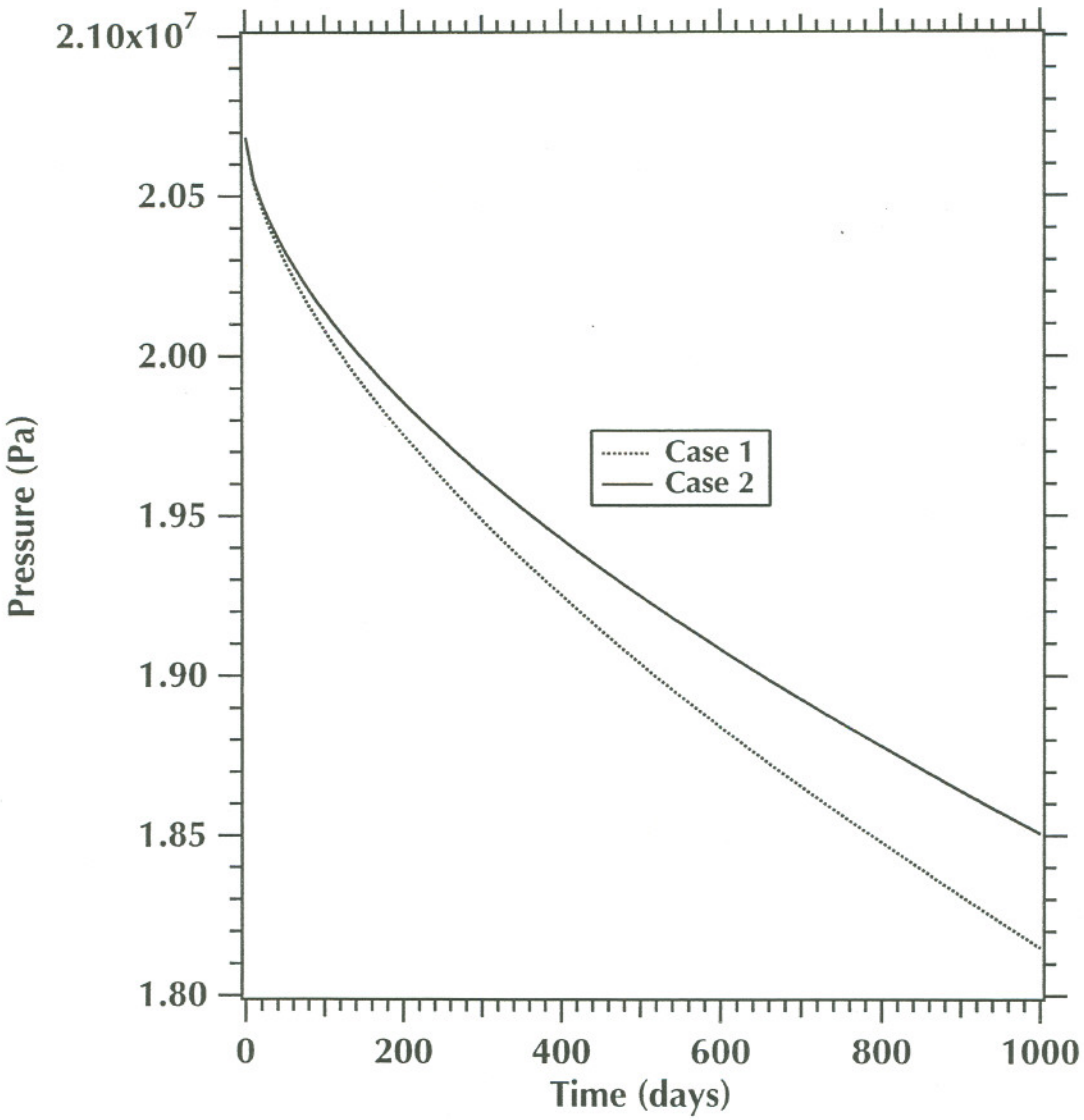

Figure 4. Test Problem 1: Pressure vs. time at the wellbore gridblock located at $r = 0.05$ m, $z = -15.05$ m.

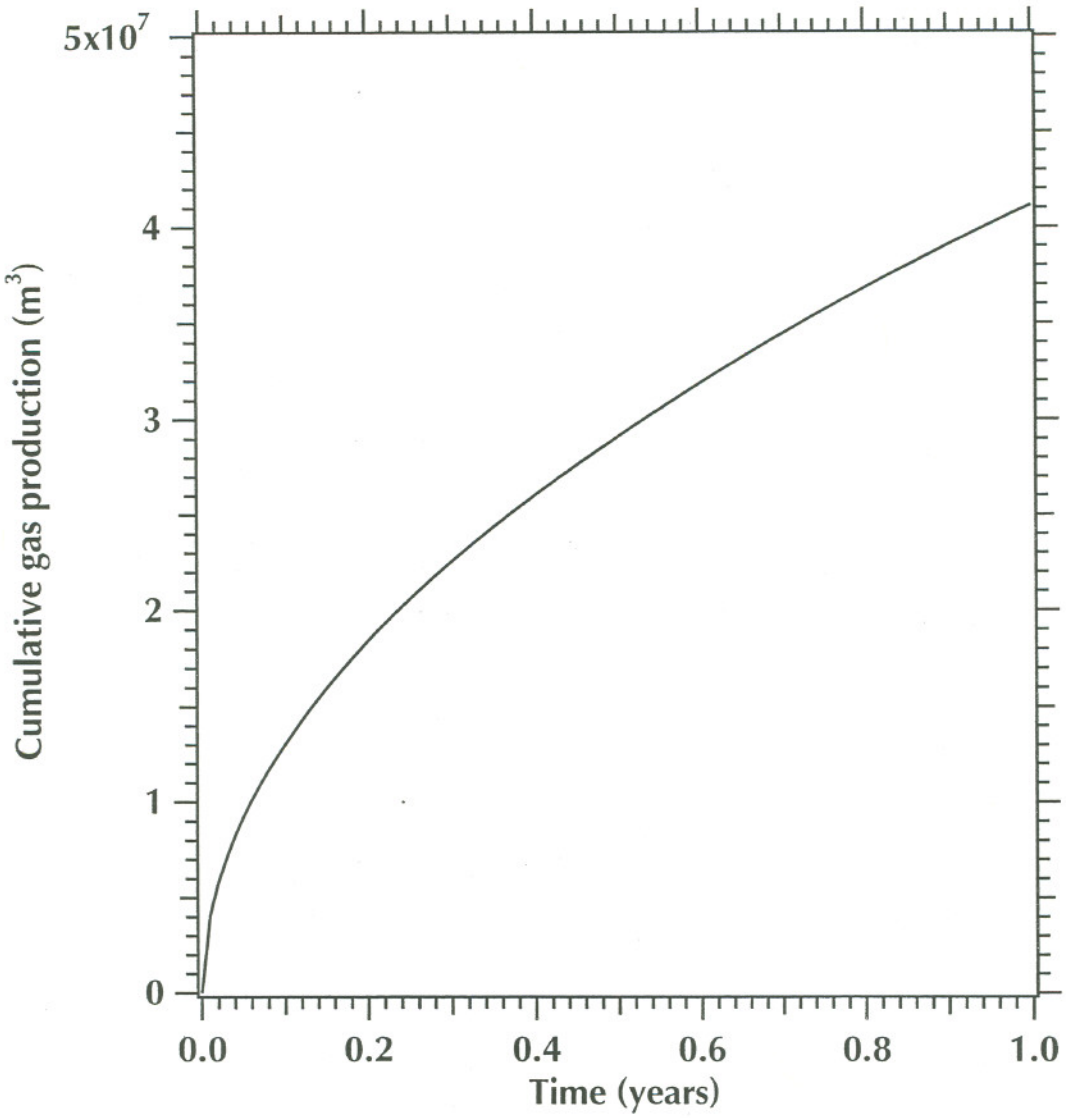

Figure 5. Cumulative CH_4 production at $t = 1$ year in Test Problem 2.

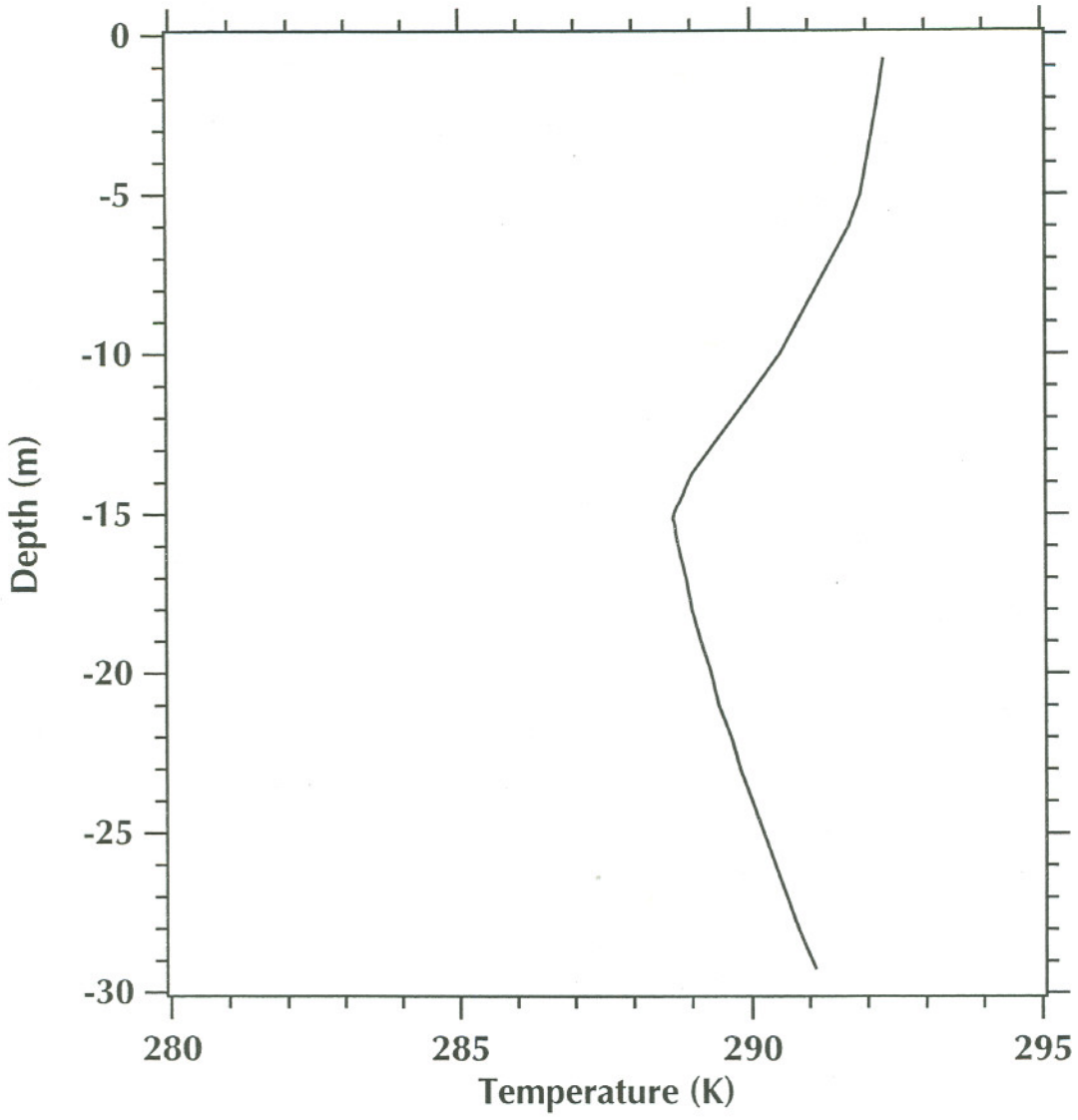

Figure 6. Vertical temperature distribution at $r = 0.15m$ in Test Problem 2.

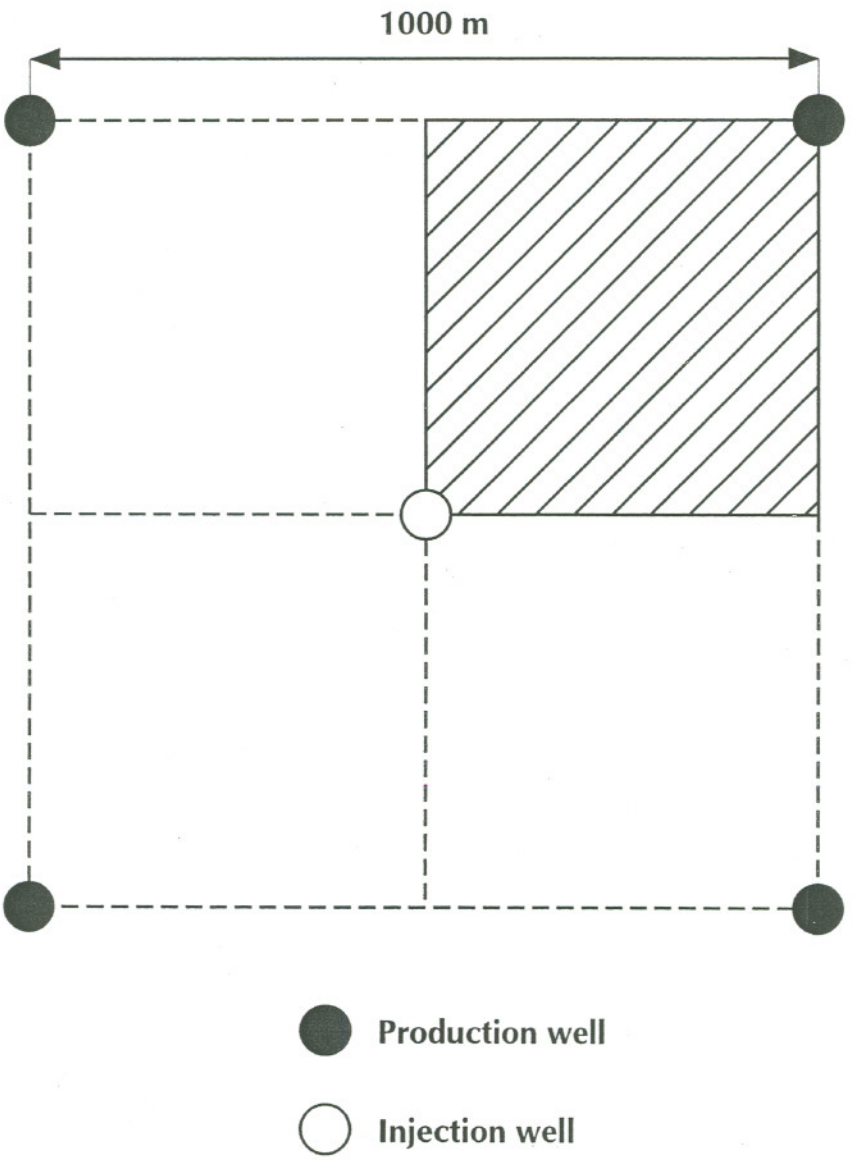

Figure 7. Five-spot well pattern for modeling a 1/4 symmetry subdomain in the frontal sweep problem.

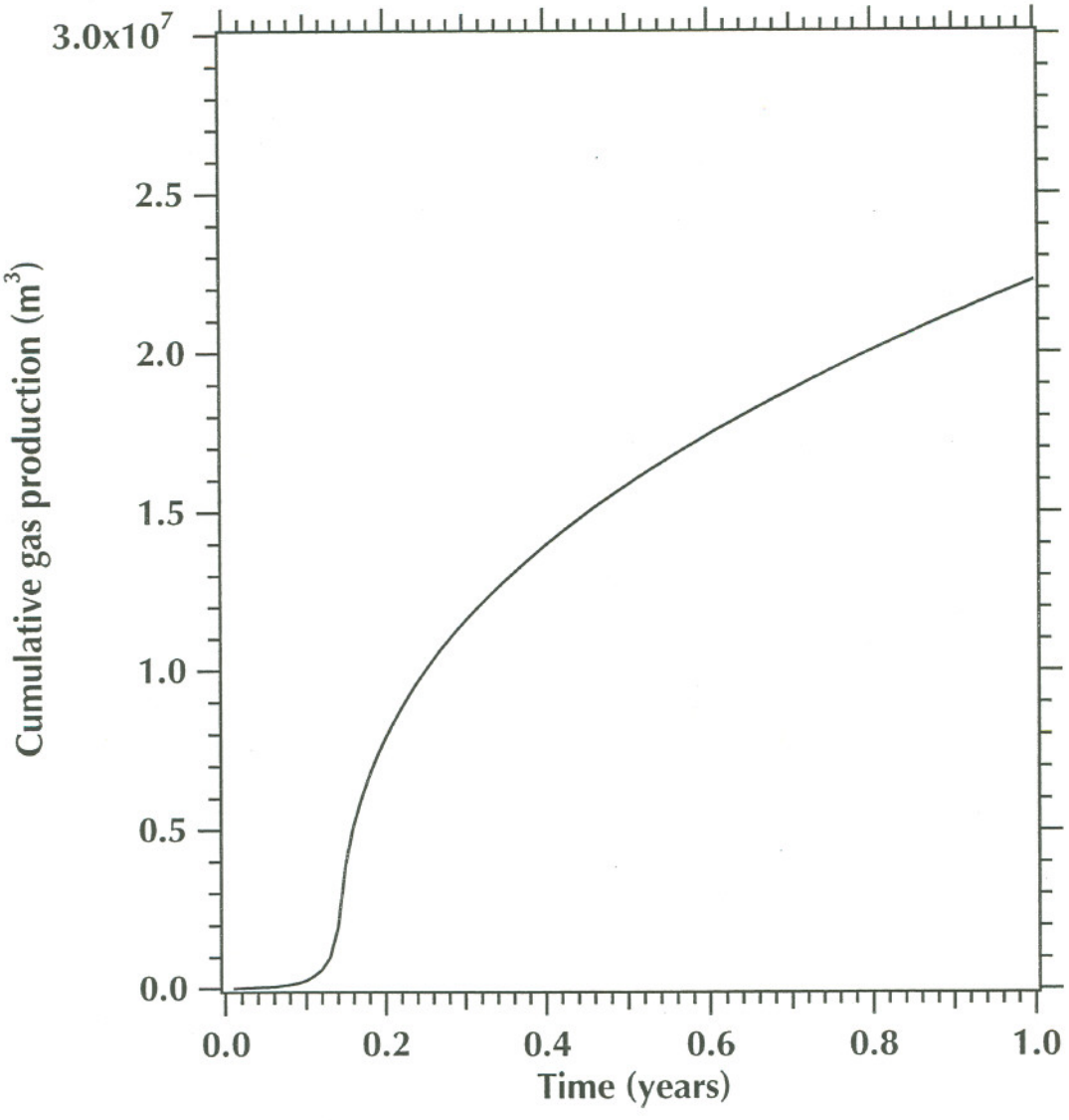

Figure 8. Cumulative CH_4 production at $t = 1$ year in Test Problem 3.

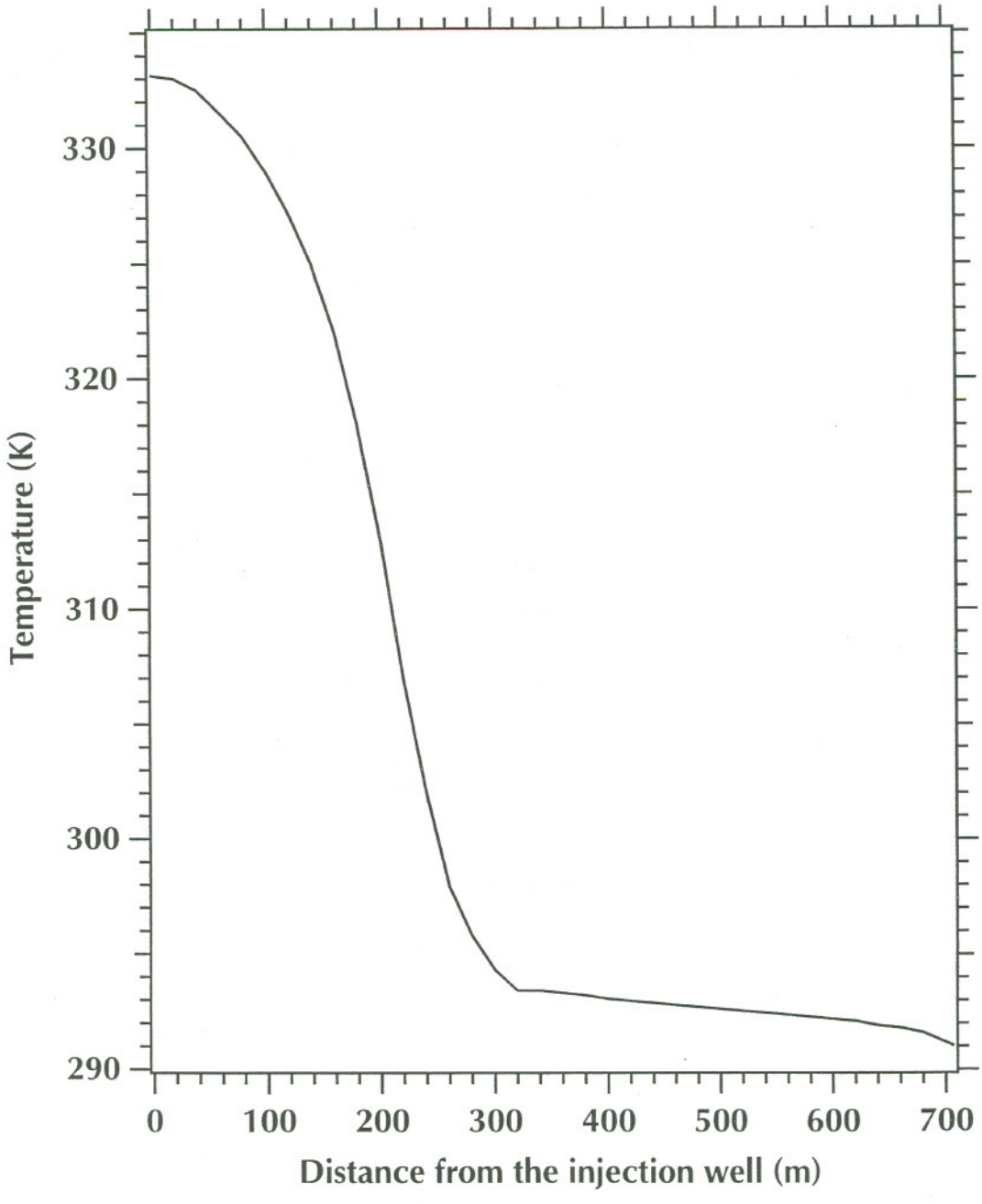

Figure 9. Temperature distribution at $t = 1$ year and at $z = -16.03$ m along the axis connecting the injection and the production wells.